RESEARCH ARTICLE

Optimizing flexibility in power systems by maximizing the region of manageable uncertainties

Aron Zingler[3] · **Stéphane Fliscounakis[4]** · **Patrick Panciatici[4]** · **Alexander Mitsos[1,2,3]**

Abstract

Motivated by the increasing need to hedge against load and generation uncertainty in the operation of power grids, we propose flexibility maximization during operation. We consider flexibility explicitly as the amount of uncertainty that can be handled while still ensuring nominal grid operation in the worst case. We apply the proposed flexibility optimization in the context of a DC flow approximation. By using a corresponding parameterization, we can find the maximal range of uncertainty and a range for the manageable power transfer between two parts of a network subject to uncertainty. We formulate the corresponding optimization problem as an (existence-constrained) semi-infinite optimization problem and specialize an existing algorithm for its solution.

Keywords Flexibility analysis · Hierarchical programming · Operation under uncertainty · Optimal power flow

1 Introduction

Uncertainty is a primal concern in the operation of power grids since exact values for supply and demand are rarely known in advance. To ensure robust grid operation, it is therefore important to quantify and improve the flexibility of a grid, i.e., the amount of uncertainty allowed in the grid while maintaining safe operation. Although assessing

✉ Alexander Mitsos
amitsos@alum.mit.edu

1 JARA-CSD, 52056 Aachen, Germany

2 Institute of Climate and Energy Systems: Energy Systems Engineering (ICE-1), Forschungszentrum Jülich GmbH, 52425 Jülich, Germany

3 Process Systems Engineering (AVT.SVT), RWTH Aachen University, 52074 Aachen, Germany

4 Réseau de transport d'électricité, Paris, France

and optimizing the flexibility of power systems is actively explored in the literature for different notions of flexibility (Nosair and Bouffard 2015; Ma et al. 2013), we want to investigate flexibility in the specific sense of an explicit measure of the range of manageable uncertain values. Manageable uncertainties are uncertainties for which operational constraints on the grid can be ensured by taking appropriate control actions. For example, a grid operator might be interested in changing generator set-points to maximize the range of power injections that can be handled by the load distribution of the grid without violating the power limit on critical lines. This perspective on flexibility seems to be underutilized in the power system literature. In contrast, this flexibility concept was already introduced in the 80 s within process systems engineering (Grossmann et al. 1983). However, as pointed out by (Wei-qing et al. 2012), the number of uncertain variables was typically small in these studies, whereas power systems applications require many variables.

We introduce a method for maximizing flexibility of power systems under uncertainty in a worst-case framework. We focus on situations where an explicit description of the region of *manageable* uncertainty is not known apriori. We allow for a two-stage approach with mixed integer control decisions. For a given parametrization of the uncertainty region, i.e., the set of all possible uncertainties, we aim to find preventive actions such that all uncertainties inside that parametrized region are manageable and the region is as large as possible. In our case studies, we use two parametrizations that allow for an intuitive interpretation of the result. In the first, we create an inner approximation of the region of manageable uncertainty by searching for the largest scaled hyperbox of uncertainties that can be managed. This allows us to find the largest amount of relative uncertainty of the node injections that can be handled. In the other, we parametrize the uncertainty region based on the amount of additional power flow from one region to another caused by the uncertainty compared to a forecasted base case. Here, the aim is to find a maximal additional power transfer capacity where every additional power flow up to the capacity is manageable.

2 Motivating example

Before discussing the general problem formulation and concrete model equations, we give a simple example of a question that can be answered using our approach. Consider the power grid instance in Fig. 1.

The lines L_i, $i = 1, 2, 3, 4$, have equal admittance h and limit P^{lim} for maximal power flow across the line.

The loads I_{c1} and I_{c2} at the two consumers $C1$ and $C2$ have predicted values I_{c1}^{pred} and I_{c2}^{pred}, but are uncertain. The loads may vary between the bounds $I_{c1} \in [I_{c1}^{pred} - \delta, I_{c1}^{pred} + \delta]$ and $I_{c2} \in [I_{c2}^{pred} - 2\delta, I_{c2}^{pred} + \delta]$. Note that the second interval is not symmetric about the predicted value I_{c2}^{pred} as the lower bound changes twice as fast compared to the upper-bound.

We want to set the set-points I_{g1}^0 and I_{g2}^0 of the two generators $G1$ and $G2$ in such a way that the predicted loads are balanced and the limits on the lines are not violated for all considered uncertain load values. To balance the difference between predicted

Fig. 1 Motivating power grid instance with two generators and two uncertain loads
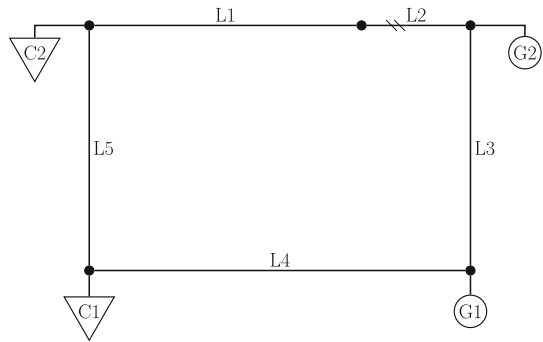
and encountered loads, we prescribe a load distribution strategy that increases the injections at both generators by the same amount, i.e., $I_{gi} = I_{gi}^0 + \Delta I_{gi}$, $i = 1, 2$ and $\Delta I_{g1} = \Delta I_{g2}$. Additionally, we can choose to open line L_2 as a control action.

As an index of flexibility, we are interested in the largest value of δ that still admits a feasible solution that is robust in the worst-case under the DC flow approximation.

In the following, we describe an approach to optimize this index, i.e., to calculate the optimal I_{gi}^0 leading to the largest corresponding δ, in this example and in more general cases.

3 Literature review

The importance of flexibility in power systems is well recognized in the literature (Babatunde et al. 2020; International Energy Agency 2011; Akrami et al. 2019). The problem of flexibility has multiple facets (Akrami et al. 2019), and the way flexibility is measured can range from "megawatts (MW) available for ramping up and down over time" (International Energy Agency 2011) over the fraction of the operating region that stays feasible when taking network limitations into account (Gómez and Borda 2019) to the "sum of probabilities of the scenarios satisfied by the chosen solution strategy" (Menemenlis et al. 2011). For the purpose of this work, we define flexibility as an explicit index that describes which values of the uncertain parameters can be handled.

We are not the first to point out the potential of this idea for power systems. In (Weiqing et al. 2012), the authors already introduce this idea of flexibility analysis from process systems to power systems. However, instead of treating uncertainty explicitly, they increase robustness with an approach that amounts to finding the maximal restriction to selected inequality constraints.

Other authors have considered the uncertainty explicitly, but evaluated the flexibility of a system without trying to optimize parameters in order to maximize it: In (Gómez and Borda 2019), the authors approximate the size of the region of manageable uncertainty but focus on cases with access to an explicit half-space representation. The authors of (Bucher et al. 2015) investigate a similar approach. They project an explicit half-space representation of the region of feasible controls for given distur-

bances into the space spanned by manageable disturbances. In (Zhao et al. 2015), the authors pursue a goal similar to ours: they determine the maximal size of a hyperbox containing manageable uncertainties while considering control actions. In contrast to their approach, we consider a general parameterization of the shape of uncertainty region and consider not only the determination but also optimization of this flexibility metric.

We aim for rigorous upper and lower bounds of our flexibility metric. As a result, our approach requires a global solution of the resulting subproblems, which becomes computationally expensive for nonlinear models. Furthermore, convergence can only be guaranteed when the grid state is uniquely defined for fixed values of preventive actions and uncertainties. We restrict ourselves to the DC flow approximation for these reasons, similarly to the references above.

The heuristic evaluation of a flexibility metric similar to ours for fixed preventive actions is investigated by Capitanescu (2021) in the context of nonconvex AC power flow. A heuristic procedure is applied that does not give any guarantees on convergence or on optimality of the result.

In (Lee et al., 2021), the authors consider the nonconvex AC power equations and construct an inner convex approximation of the feasible region around an initial point under uncertainty. For uncertainty, they consider uncertain power injections y that are known to occur in an ellipse around a nominal point y^0 with a given radius γ. As one application, they consider finding locally the maximum robustness margin, which is the size of the uncertainty set against which the solution is robust, i.e., the maximum radius γ. This is the only publication known to us that also considers taking actions to optimize the flexibility of the network in a way that allows for an interpretation of the result in terms of manageable uncertainty values.

4 Problem formulation and solution

In our general problem formulation, we maximize a scalar index for flexibility δ by adjusting preventive actions for grid operation $x \in \mathcal{X}$. The flexibility index δ determines the size of the parametric uncertainty region $\mathcal{T}(\delta, x)$. We must guarantee the existence of controls $z \in \mathcal{Z}(x, y)$ that allow safe grid operation, captured by a continuous inequality constraint g^s, for all uncertainty values $y \in \bar{\mathcal{Y}}$ in the parametric uncertainty region $\mathcal{T}(\delta, x)$, as well as for a predicted state with fixed y^0 and z^0. We assume that the grid states are uniquely given by a continuous function $s(x, y, z)$ and that the set of controls $\mathcal{Z}(x, y)$ is not empty on $\mathcal{X} \times \bar{\mathcal{Y}}$.

The resulting problem

$$
\inf_{\delta \in \mathbb{R}^+, x \in \mathcal{X}} - \delta
$$
$$
\text{s.t. } g^s(x, y^0, z^0, s(x, y^0, z^0)) \leq 0, \tag{1}
$$
$$
\forall y \in \mathcal{T}(\delta, x) \left[\exists z \in \mathcal{Z}(x, y) : \ g^s(x, y, z, s(x, y, z)) \leq 0 \right]
$$

is a generalized existence-constrained semi-infinite optimization problem. In our case, the model is based on the DC flow approximation (which will lead to MILP subproblems) and introduced next together with our choices for the preventive actions x, the uncertainties y and the controls z. In this context, the function s is not known explicitly but is rather given implicitly by the model constraints. To solve this challenging problem, we specialize the discretization algorithm from (Djelassi and Mitsos 2021), which allows for the inclusion of the implicit function s (Djelassi et al. 2019).

5 Model equations

This work builds upon the model described in (Djelassi et al. 2018; Djelassi 2020). An overview of the model is given below. For a complete description, we refer to the aforementioned references.

5.1 Notation

The power grid topology is represented by a directed graph with nodes $n \in \mathcal{N}$ and edges $e \in \mathcal{E}$. Each edge e has an originating node $\tilde{n}(e)$ and a terminating node $\tilde{m}(e)$. Each node n has a set of incoming edges $\mathcal{E}^+(n)$ and outgoing edges $\mathcal{E}^-(n)$. Some of the nodes are connected to generators $g \in \mathcal{G}$. We denote this set of generator nodes $\mathcal{N}_G \subseteq \mathcal{N}$ and the mapping of generators to corresponding nodes as $n_G(g)$. Some of the edges are associated with a phase-shifting transformer (PST). The corresponding set of shifter edges is denoted by $\mathcal{E}_S \subseteq \mathcal{E}$.

5.2 Summary of the model

In the general formulation (1), we differentiate between preventive actions x and control actions z. They differ in the following way: The preventive actions x have to be selected in a first stage without prior knowledge of the uncertainty values y. In our model, the preventive actions are the set points for power generated by the generators $x^T = [I_1^x, ..., I_{|G|}^x]^T$.

The value of the flexibility index δ also has to be selected in the first stage. It determines how much we restrict the uncertainty values that can occur in the second stage. Higher values of δ increase the size of the parametric uncertainty region $\mathcal{T}(\delta, x)$ but also improve the value of the objective function.

In the second stage, worst-case uncertainty values y are determined within the parametric uncertainty region $\mathcal{T}(\delta, x)$. They consist of the uncertain derivations for the nodal power injections ΔI_n^y from their predicted values I_n^0 at nodes $n \in \mathcal{N}$, i.e., $y^T = [\Delta I_1^y, ..., \Delta I_{|\mathcal{N}|}^y]^T$.

The control variables z are chosen in the last stage with full knowledge of the uncertainty values. They include the setting of phase shifter m_e on the edges $e \in \mathcal{E}$ and binary decision variables p_b that decide if designated pairs of busses $b \in \mathcal{B}$ are merged. In other words, $z^T = [\Delta \theta_1, ..., \Delta \theta_{|\mathcal{E}|}, p_1, ..., p_{|\mathcal{B}|}]^T$.

Fig. 2 Illustration of the behavior of phase shifters
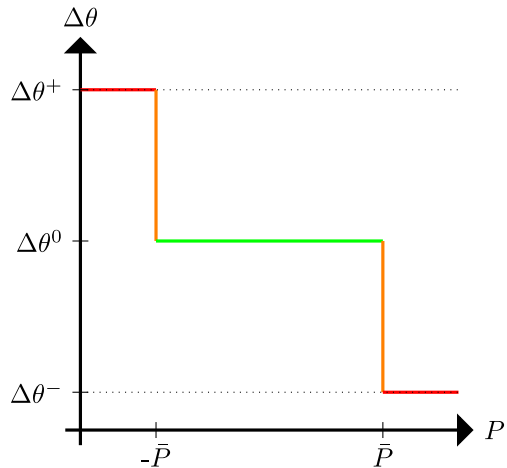
We also consider a fixed load distribution scheme among the generators. The power generation at the generators can be changed by control offsets ΔI_g^z at generators $g \in \mathcal{G}$. Those offsets are conceptually control decisions. However, as detailed later, because they are uniquely determined as a function of the uncertainty offsets for the nodal power injections ΔI_n^y and the generator set points I_g^x, we should calculate them alongside the uncertainty values (Djelassi et al. 2019).

The vector of implicit state variables s contains the voltage angles at nodes $n \in \mathcal{N}$, denoted as θ_n, and the $s = [\theta_1, ..., \theta_{|\mathcal{N}|}]$. The implicit state variables are given uniquely by the implicit function $s(x, y, z)$, i.e., they are determined by the other variables and the grid equations.

5.3 Components

5.3.1 Edges

To calculate the power flow P_e over an edge $e \in \mathcal{E}$, the DC power flow approximation

$$P_e = h_e(\theta_{\tilde{n}(e)} - \theta_{\tilde{m}(e)} + \Delta\theta_e) \tag{2}$$

is used with the positive admittance h_e, the voltage angle of the originating node $\theta_{\tilde{n}(e)}$ and the voltage angle of the terminating node $\theta_{\tilde{m}(e)}$. The phase shift $\Delta\theta_e$ is zero for all edges $e \in \mathcal{E}\backslash\mathcal{E}_S$ without a PST. For the edges with a PST, the phase-shift of a PST only deviates from zero if the magnitude of power flow $|P_e|$ reaches or exceeds a specified activation threshold $\bar{P}$. The phase-shift will vary in its bounds, i.e., $[\Delta\theta_e^-, \Delta\theta_e^+]$ to keep the power flow from exceeding the limit until this is prevented by said bounds. This piecewise linear model was introduced in (Djelassi et al. 2018) to reduce unrealistic continuous control in the PST and is illustrated in Fig. 2.

An additional control mechanism is given by bus merging. For a predefined set of pairs of nodes $\mathcal{B} \subseteq \mathcal{N} \times \mathcal{N}$, we allow a single pair to be merged. For each pair

$b \in \mathcal{B}$, the binary variable p_b encodes if the pair of nodes is merged. We can model bus merging with a line that has infinite admittance if closed but can also be open. Thus, for these lines, we can model their behavior with the following disjunction:

$$p_b = 0 \implies 0 = P_b$$
$$p_b = 1 \implies 0 = \theta_{\tilde{n}(b)} - \theta_{\tilde{m}(b)}$$

5.3.2 Nodes

The injection I_n at a any node $n \in \mathcal{N}$ must equal the outgoing power-flows over the connected edges

$$I_n = \sum_{e \in \mathcal{E}: n = \tilde{n}(e)} P_e - \sum_{e \in \mathcal{E}: n = \tilde{m}(e)} P_e. \tag{3}$$

The injection I_n at non-generator nodes $n \in \mathcal{N} \backslash \mathcal{N}_G$ is uncertain and given by

$$I_n = I_n^0 + \Delta I_n^y \tag{4}$$

with an initial injection of I_n^0 and an uncertainty offset ΔI_n^y within given bounds ($\Delta I_n^y \in [\Delta I_n^{y-}, \Delta I_n^{y+}]$).

The injection I_n at nodes $n = n_G(g)$ with generators $g \in \mathcal{G}$ is given by

$$I_{n_G(g)} = I_{n_G(g)}^0 + I_g^x + \Delta I_g^z + \Delta I_{n_G(g)}^y \tag{5}$$

where I_g^x is injection by the generator g at its set point and ΔI_g^z is the control offset due to load distribution.

The control offset of generators follows a piecewise linear profile. The sum of all injections due to control offsets must cancel the additional injections due to uncertainty. In total, the total injection demand

$$\Delta I^t = -\sum_{n \in \mathcal{N}} \Delta I_n^y = \sum_{g \in \mathcal{G}} \Delta I_g^z \tag{6}$$

must be injected by load distribution.

Ideally, this total injection would be divided among the generators $g \in \mathcal{G}$ according to a contribution factor $c_g \geq 0$ with $\sum_{g \in \mathcal{G}} c_g = 1$. However, the demanded control offset $\Delta I_g^{z,dem} = c_g \Delta I^t$ at each generator $g \in \mathcal{G}$ can be prohibited because the total generator output is limited by the generator bounds I_g^{x-} and I_g^{x+}, i.e.,

$$I_g^{x-} \leq I_g^x + \Delta I_g^z \leq I_g^{x+}. \tag{7}$$

In this situation, we introduce an artificially increased total injection demand $\Delta I^{t,inc}$ such that the control offsets resulting from this increased total injection demand and

Fig. 3 Illustration of the behavior of generator g
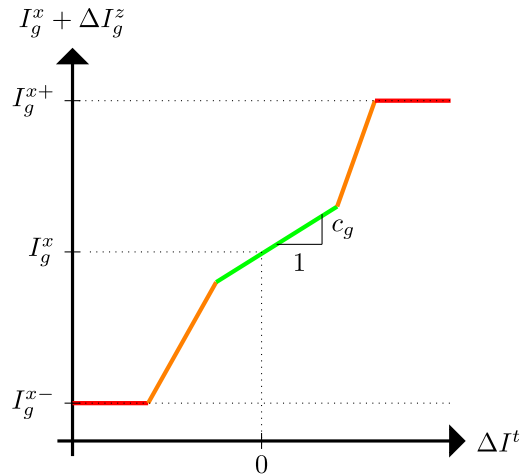
the limits on generator output fulfill

$$\Delta I^t = \sum_{g \in \mathcal{G}} \underbrace{\mathrm{mid}(I_g^{x-}, I_g^x + c_g \Delta I^{t,inc}, I_g^{x+}) - I_g^x}_{\Delta I_g^z}. \tag{8}$$

Here, the mid function returns the median of its elements.

As a result, generators will increase their injections at a faster rate once some of the other generators have reached their injection limits. The resulting behavior of the generator injection is visualized in Fig. 3.

It is difficult to provide an explicit description of the control offset ΔI_g^z at generator g as a function of the uncertainty offsets ΔI_n^y for nodes $n \in \mathcal{N}$ and the generator set points $I_{\bar{g}}^x$ for generators $\bar{g} \in \mathcal{G}$. However, as long as the load distribution control is feasible, i.e., we assume

$$\sum_{g \in \mathcal{G}} -I_g^{x+} \le \sum_{n \in \mathcal{N}} I_n^0 + \Delta I_n^y \le \sum_{g \in \mathcal{G}} -I_g^{x-}, \tag{9}$$

this model for the load distribution implicitly sets the control offsets to unique values. This is an important characteristic of the model because it means that the control actions z do not include any degree of freedom regarding the injections of the network.

6 Algorithm

Our algorithm is based on an algorithm (Djelassi and Mitsos 2021) that is suitable for the global solution of so-called existence-constrained semi-infinite optimization problems (ESIPs) with continuous nonlinear functions. We show that (1)

can be formulated as an ESIP and specialize the algorithm based on some of the properties of (1). In the following discussion, we will use $g(x, y, z) := \max \left\{ g^s(x, y, z, s(x, y, z)), g^s(x, y^0, z^0, s(x, y^0, z^0)) \right\}$ to shorten the notation.

6.1 Reformulation to an existence constrained semi-infinite optimization problem

Problem (1) is a slight generalization of an existence-constrained semi-infinite optimization problem (ESIP), which have the form

$$\inf_{\check{x} \in \mathcal{X}} \check{f}(\check{x}) \text{s.t.} \ \forall \check{y} \in \check{\mathcal{T}} \left[\exists \check{z} \in \check{\mathcal{Z}}(\check{x}, \check{y}) : \check{g}(\check{x}, \check{y}, \check{z}) \leq 0 \right] \tag{10}$$

and for which a global solution procedure was presented in (Djelassi and Mitsos 2021).

The problem (1) is a generalization in the sense that the uncertainty domain $\mathcal{T}(x, \delta)$ is parametric in the preventive actions, while $\check{\mathcal{T}}$ in (10) is constant. However, the following proposition shows that we can use a commonly used relaxation to remove the dependency of the uncertainty domain on preventive actions. Furthermore, this relaxation is exact in our application in the sense that the infimum of (12d) is the same as the minimum of the relaxation.

Proposition 1 *Assume that the uncertainty domain is defined by a continuous function h in the form $\mathcal{T}(x, \delta) := \{y \in \bar{\mathcal{Y}} | h(x, y) \leq \delta\}$ with a given host set for the uncertain values $\bar{\mathcal{Y}}$. We can exactly reformulate problem (1) to a problem with fixed uncertainty set by replacing the constraint*

$$\forall y \in \mathcal{T}(\delta, x)[\exists z \in \mathcal{Z}(x, y) : g(x, y, z) \leq 0] \tag{11}$$

with

$$\forall y \in \bar{\mathcal{Y}}[\exists z \in \mathcal{Z}(x, y) : \min \{\alpha (\delta - h(x, y)), g(x, y, z)\}]$$

for any arbitrarily chosen but fixed scaling constant $\alpha \in \mathbb{R}^+$.

Proof We reformulate the constraint for the preventive actions x and the flexibility index δ in problem (1), i.e., (11) in the following way:

$$\forall y \in T(x, \delta) \left[\exists z \in \mathcal{Z}(x, y) : g(x, y, z) \leq 0 \right] \tag{12a}$$

$$\Leftrightarrow \forall y \in T(x, \delta) \left[\min_{z \in \mathcal{Z}(x, y)} g(x, y, z) \leq 0 \right] \tag{12b}$$

$$\Leftrightarrow \forall y \in \bar{\mathcal{Y}} \left[\delta < h(x, y) \vee \min_{z \in \mathcal{Z}(x, y)} g(x, y, z) \leq 0 \right]. \tag{12c}$$

We relax the strict inequality and obtain

$$\forall y \in \bar{\mathcal{Y}} \left[\delta \leq h(x, y) \vee \min_{z \in \mathcal{Z}(x, y)} g(x, y, z) \leq 0 \right]. \tag{12d}$$

which in turn is equivalent to

$$\forall \boldsymbol{y} \in \bar{\mathcal{Y}} [\min_{\boldsymbol{z} \in \mathcal{Z}(\boldsymbol{x}, \boldsymbol{y})} \min \{\alpha \left(\delta - h(\boldsymbol{x}, \boldsymbol{y})\right), g(\boldsymbol{x}, \boldsymbol{y}, \boldsymbol{z})\} \leq 0] \tag{12e}$$

$$\Leftrightarrow 0 \geq \sup_{\boldsymbol{y} \in \bar{\mathcal{Y}}} \min_{\boldsymbol{z} \in \mathcal{Z}(\boldsymbol{x}, \boldsymbol{y})} \min \{\alpha \left(\delta - h(\boldsymbol{x}, \boldsymbol{y})\right), g(\boldsymbol{x}, \boldsymbol{y}, \boldsymbol{z})\} \tag{12f}$$

$$\Leftrightarrow \forall \boldsymbol{y} \in \bar{\mathcal{Y}} [\exists \boldsymbol{z} \in \mathcal{Z}(\boldsymbol{x}, \boldsymbol{y}) : \alpha \min \{\delta - h(\boldsymbol{x}, \boldsymbol{y}), g(\boldsymbol{x}, \boldsymbol{y}, \boldsymbol{z})\} \leq 0] \tag{12g}$$

for any arbitrary scaling constant $\alpha \in \mathbb{R}^+$.

It remains to show that the relaxation from (12c) to (12d) is exact in this specific case, in the sense that the infimum of (1) is the same as the minimum of the relaxation. To see this, consider any solution $(\delta, \boldsymbol{x})$ fulfilling the relaxation (12d). For any $\epsilon > 0$ the disturbed solution $(\delta - \epsilon, \boldsymbol{x})$ fulfills the original constraint (12c) and is thus feasible in the original problem. If the point $(\delta, \boldsymbol{x})$ was a global minimizer in the relaxation, the corresponding objective value is δ. The objective value of the disturbed solution is $\delta - \epsilon$. As ϵ goes to zero, the relaxation only introduces an arbitrarily small error in the objective function value obtained.

Note that the set of uncertainties is now $\bar{\mathcal{Y}}$ and does no longer vary with the preventive actions $\boldsymbol{x}$. Consequently, we can use existing algorithms for ESIPs.

6.2 Algorithmic steps

We employ an adaptive discretization approach. The fundamental idea is to iteratively add worst-case scenarios for the values of the uncertain variables and dates back to (Blankenship and Falk 1976).

In (Djelassi and Mitsos 2021), we detailed how to extend our previous algorithm from (Djelassi and Mitsos 2017) for standard semi-infinite optimization problems to ESIPs. The extended algorithm used there is a modification of our restriction of the right-hand side algorithm for semi-infinite optimization problems (Mitsos 2011).

Instead of the modified algorithm, we use the restriction of the right-hand side algorithm as the basis here because it is easier to parallelize. We believe it is necessary to use parallelization and focus on wall run time because, in application, we might start the calculation based on current information, and we expect that the uncertainty compared to the nominal state increases as time passes.

The algorithm uses two subproblems, the upper-level and the lower-level problem. In the upper-level problem, we solve

$$\min_{\delta \in \mathbb{R}^+, \boldsymbol{x} \in \mathcal{X}, \boldsymbol{z}^1, \ldots, \boldsymbol{z}^{|\mathcal{D}|}} -\delta$$
$$\text{s.t. } \forall d \in \mathcal{D} : \min \left\{\alpha \left(\delta - h(\boldsymbol{x}, \boldsymbol{y}^d)\right), g(\boldsymbol{x}, \boldsymbol{y}^d, \boldsymbol{z}^d)\right\} \leq -\epsilon_R \tag{13}$$
$$\forall d \in \mathcal{D} : \boldsymbol{z}^d \in \mathcal{Z}(\boldsymbol{x}, \boldsymbol{y}^d)$$

for a given discretization $\mathcal{Y}^{disc} = \{y^d, d \in \mathcal{D}\}$ with index set $\mathcal{D}$ and restriction $\epsilon_R > 0$. We run two procedures in parallel. In the lower-bounding procedure, we set the restriction ϵ_R to zero, which means that every objective value of (13) is an update to the lower bound $-\delta^{LB}$ for (1). We also run an upper-bounding procedure that uses positive values of ϵ_R, starting from ϵ_R^0, in order to find a feasible solution (and thus an update to the upper bound $-\delta^{UB}$). Using the scheme to iteratively reduce ϵ_R (by a constant factor $\frac{1}{r_R}$) introduced in (Mitsos 2011), a feasible and ϵ-optimal solution can be found in finitely many steps.

In both procedures, we also solve a worst-case generation problem, which is represented by the right-hand-side of (12f). In the worst-case generation problem, we solve for the worst-case uncertainty values for given values of δ and x. If the worst-case generation problem has a positive maximal objective value, it provides the next addition to the discretization $\mathcal{Y}^{disc}$. Otherwise, it confirms the feasibility of the pair (x, δ).

The worst-case generation problem (12f) is a maxmin problem and is solved via a discretization approach for minmax problems (Falk and Hoffman 1977). This solution approach for the worst-case generation problem is similar to the procedure outlined above. However, we do not require an analog to the upper-bounding procedure since the objective value of the inner minimization problem already provides the required bound (Falk and Hoffman 1977).

6.3 Specialization

We specialize the algorithm with three changes. The first two aim to exploit the special case where $\mathcal{T}(x, \delta) = [y^0 - \mathbf{\Delta}^- \delta, \, y^0 + \mathbf{\Delta}^+ \delta] \subseteq \bar{\mathcal{Y}}$, which is a scaled hyperbox around a nominal point y^0 with fixed scaling factor vectors $\mathbf{\Delta}^+$ and $\mathbf{\Delta}^-$. The other provides an additional way of finding an upper bound.

6.3.1 Dropping redundant discretization points

When the parametric uncertainty region does not depend on the preventive actions x, i.e., $\mathcal{T}(x, \delta) = \tilde{\mathcal{T}}(\delta) := \{y \in \bar{Y} | \tilde{h}(y) \geq \delta\}$, we can reduce the size of the optimization problem (13), by removing points y^d with $\tilde{h}(y^d) \geq \delta^{LB}$ for the following iterations. Indeed, with the information $\delta \leq \delta^{LB}$, these discretization points are redundant. Note that each discretization point increases the problem size not only due to the additional constraints but also due to the additional decision variables z^d added to the problem.

6.3.2 Transformation-based reformulation

As mentioned above, discretization points become redundant when the lower bound satisfies $\tilde{h}(y^d) \geq \delta^{LB}$. Similar behavior occurs during the solution of (13). Because we maximize δ, its value will only fall below $h(y^d)$ if there are no preventive actions x and controls z^d with $g(x, y^d, z^d) \leq 0$. However, if δ falls below $h(y^d)$, the discretization point has no further influence. In the specific case of a scaled hyperbox,
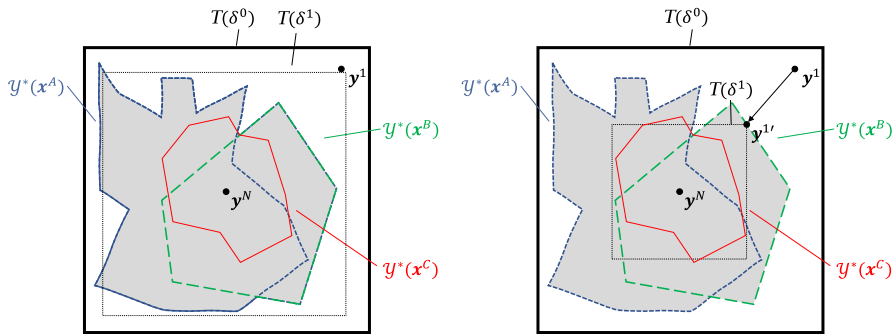
(a) Behavior of the algorithm without the transformation. The original box $\mathcal{T}(\delta^0)$ (thick black line) is reduced so that the discretization point y^1 is outside of the new box $\mathcal{T}(\delta^1)$ (dotted line).

(b) Behavior of the algorithm with the transformation. The discretization point y^1 is projected on the boundary of the box. The box must be reduced until the transformed point $y^{1'}$ can be handled with one of the choices for the preventive actions (gray area). The resulting box $\mathcal{T}(\delta^1)$ (finely dotted line) is smaller.

Fig. 4 Illustration of the behavior of the algorithm with and without transformation in a fictitious example. $\mathcal{Y}^*(x)$ denotes the set of all uncertainty values y that can be handled with the preventive actions x. None of the preventive actions x^A, x^B, x^C can handle the discretization point y^1

i.e., $\tilde{T}(\delta) = [y^0 - \mathbf{\Delta}^-\delta, y^0 + \mathbf{\Delta}^+\delta] \subseteq \bar{\mathcal{Y}}$, this would mean that a discretization point y^d will be ignored if the hyperbox is reduced enough to exclude it. This is shown in Fig. 4a. However, we can still utilize the discretization point by using a transformation. Specifically, we choose to transform it so that it traces a path from the border of the hyperbox instead of being ignored by using

$$\min_{\delta \in \mathbb{R}^+, x \in \mathcal{X}, z^1, \dots, z^{|\mathcal{D}|}} -\delta$$

$$\text{s.t. } \forall d \in \mathcal{D} : g\left(x, y^0 + (y^d - y^0)\frac{\min\{h(y^d), \delta\}}{h(y^d)}, z^d\right) \leq -\epsilon_R \qquad (14)$$

$$\forall d \in \mathcal{D} : z^d \in \mathcal{Z}(x, y^d)$$

instead of (13). This is visualized in Fig. 4b. When using this transformation, we can choose to drop the discretization points as mentioned above, but it can also be beneficial to keep them. Similar transformations are known in the context of generalized semi-infinite programming (Still 1999). A similar idea has also been discussed in (Zhao et al. 2022) in the context of flexibility index evaluation without discretization-based methods. The expected benefit of using this reformulation is reducing the total number of necessary iterations by reducing δ further in a single iteration.

6.3.3 Upper-bounding heuristic

In the procedure described, an upper bound is found when the upper or lower-bounding procedure produces a pair (x, δ) that is feasible, i.e., fulfills (12f). Note that (13) can

return a pair of preventive actions x and flexibility index δ, which is infeasible but would be feasible for a reduced δ. Also note that we can rewrite the feasible region of (12f) for fixed preventive actions x as a constraint on the flexibility index

$$\delta \leq \inf_{y \in \bar{\mathcal{Y}}} h(x, y)$$
$$\text{s.t. } \min_{z \in \mathcal{Z}(x,y)} g(x, y, z) > 0. \tag{15}$$

Solving the problem on the right-hand side of the inequality of (15), we can find $-\delta_{wc}(x)$, a tight upper-bound on our objective value in (1), $-\delta$, for fixed preventive actions x. A similar problem for finding the flexibility index for fixed preventive actions x in a more restricted setting appears in (Grossmann and Floudas 1987). In our setting, finding the flexibility index for fixed preventive actions x, i.e., solving (15), is only used as a subproblem but has useful applications on its own. Variants of this problem are discussed in the power flow literature; see, for example, (Zhao et al. 2015; Capitanescu 2021). When the strict inequality is relaxed, this problem is a semi-infinite optimization problem. In our test cases, we again use the restriction of the right-hand side algorithm from (Mitsos and Tsoukalas 2015) to solve this relaxed problem. Since we relax problem (15), we do not necessarily obtain the tight upper-bound $-\delta_{wc}(x)$, but a pessimistic value $-\delta_{wc}^{relax}(x) \geq -\delta_{wc}(x)$. This procedure is started in parallel when new preventive actions x are encountered in either the lower or upper-bounding procedure.

7 Parametric uncertainty region formulations

A key aspect in choosing the parametrization of the uncertainty region $\mathcal{T}(x, \delta)$ is the interpretability of the resulting value of δ. To illustrate the potential uses of the formulation (1), we investigate two parametrizations for the uncertainty region in the context of flexibility of power grids. They differ mainly in the choice of the parametric uncertainty region $\mathcal{T}(x, \delta)$. In both cases, the value of δ has a specific interpretable meaning.

7.1 Inner approximation of region of manageable uncertain injections with a scaled hyperbox

In this case, we are given the forecasted uncertain injections y^0 and scaling vectors Δ^- and Δ^+ for the expected positive and negative deviation from that forecast, respectively. We are also given an initial known upper bound for the flexibility δ^{UB} that defines the host set for the uncertainties $\bar{\mathcal{Y}}$. We search for the largest flexibility index δ and decision variables x (representing generator set-points), such that all uncertain injections $\tilde{T}(\delta) = [y^0 - \Delta^- \delta, y^0 + \Delta^+ \delta]$ can be handled while ensuring that the power flow P_e over on the critical edges $e \in \mathcal{E}_c$ does not exceed a specified limit P_e^{lim},

i.e., g represents the constraints

$$|P_e| \leq P_e^{lim}, \quad \forall e \in \mathcal{E}_c \tag{16}$$

which we can summarize as the scalar constraint

$$\max_{e \in \mathcal{E}_c} \frac{|P_e|}{P_e^{lim}} - 1 \leq 0. \tag{17}$$

The resulting hyperbox will constitute an inner approximation of the region of all manageable uncertain injections. Its size is maximized by the returned preventive actions $\boldsymbol{x}$. A possible application of this parametrization is to search for the maximal uncertainty of node injections relative to the initial or forecasted injections.

7.2 Maximal available net power transfer capacity

We also investigate the problem of finding maximal additional power transfer capacity δ from a region A to a region B of the network. We assume that we are given a range for potential uncertain injections, i.e., $\bar{\mathcal{Y}} = [\boldsymbol{y}^-, \boldsymbol{y}^+]$ and forecasted values $\boldsymbol{y}^0$. For the found power transfer capacity δ, we must guarantee nominal grid operations, i.e., (17), for any realization of the uncertainty that leads to an additional net power transfer within $[0, \delta]$ from region A to a region B. Note that this differs from finding the maximal additional power transfer δ^{max} that can be safely achieved under the specified uncertainty, as this would not guarantee that *all* power transfers $\delta^\dagger$ with $0 \leq \delta^\dagger < \delta^{max}$ can be archived safely.

We formulate this as follows: We denote with $\mathcal{N}_A$ and $\mathcal{N}_B$ the sets of nodes inside the regions A and B regions and with $\mathcal{G}_A$ and $\mathcal{G}_B$ the generators within these regions, respectively. The additional net power transfer is the minimum of the additional injections in the A region and the decrease of injections in the B region. As a result, the function h describing the uncertainty region takes the form

$$h(\boldsymbol{x}, \boldsymbol{y}) = \min \left\{ \sum_{n \in \mathcal{N}_A} I_n - I_n^0 - \sum_{g \in \mathcal{G}_A} I_g^x, \sum_{n \in \mathcal{N}_B} -I_n + I_n^0 + \sum_{g \in \mathcal{G}_B} I_g^x \right\}. \tag{18}$$

Since we only need to handle uncertainty values $\boldsymbol{y}$ resulting in positive flows from A to B, the constraint g takes the form

$$\min\{\alpha h(\boldsymbol{x}, \boldsymbol{y}), \max_{e \in \mathcal{E}_c} \frac{|P_e|}{P_e^{lim}} - 1\} \leq 0 . \tag{19}$$

Note that, as mentioned earlier, the control offsets for generators $g \in \mathcal{G}$ are uniquely determined by the generator set points I_g^x at all generators $g \in \mathcal{G}$ (included in the preventive actions $\boldsymbol{x}$) and the additional injections ΔI_n^y at all nodes $n \in \mathcal{N}$ (included in the uncertain values $\boldsymbol{y}$). As a result, the injections I_n for $n \in \mathcal{N}$ are not a function
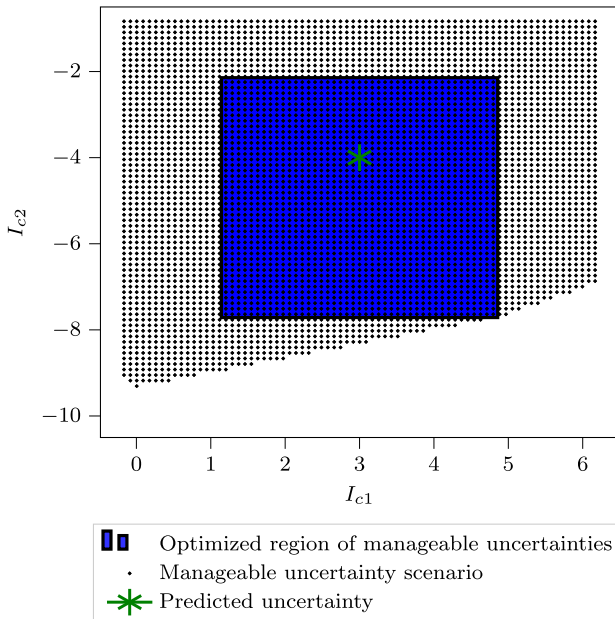
Fig. 5 Visualization of the result from the motivating example for the final preventive actions. The optimized region of manageable uncertainties is valid and optimal for the chosen parameterization

of the control variables z. Therefore, the net flow between the regions as defined by (18) is also independent of the control variables z.

8 Numerical experiments

We now report results from numerical experiments for both parametric uncertainty region formulations on a small-scale instance based on the modified 30-bus IEEE system from (Djelassi et al. 2018) and a medium-scale grid instance generated at RTE.

All computations are run on a system with a Skylake Platinum 8160 processor using 24 cores and 48GB of memory. To solve the resulting mixed-integer optimization problems, we use Gurobi 10.0.2. Each instance of the MILP solver is allowed to use up to 6 threads. For the medium-sized instance, numerical problems were caused on some runs by integrality violations. Instead of reducing the integrality tolerance from its default value, we used the *IntegralityFocus* setting in Gurobi. We use a relative optimality tolerance of 0.05 for the overall algorithm and 0.025 for the auxiliary problem (15). The initial restriction ϵ_R^0 is set to 0.05 for the overall algorithm and 0.005 for the auxiliary problem. In both cases, we use $r_R = 2$ to determine the reduction rate of the restriction ϵ_R.

For the parametrization from Sect. 7.1, we use the largest number that guarantees (9) as the initial upper bound δ^{UB}.

Table 1 Properties of the small grid instance

Nodes	Generators	Edges	Shifters	Critical edges	Bus merges
37	6	41	3	41	7

8.1 Motivating example

We solve the motivating example from Sect. 2 with the parameters $h = 1$S, $P^{lim} = 5$M W $I_{c1}^{pred} = 3$M W, $I_{c2}^{pred} = -4$M W and $I_{g1} \in [-7.5\text{M W}, 3\text{M W}]$, $I_{g2} \in [-3\text{M W}, 7.5\text{M W}]$. Here, we are interested in the uncertainty parameterization as a scaled hyperbox from Sect. 7.1. Note that the scaling vectors given in the description of the example are $\boldsymbol{\Delta}^+ = [1, 1]^T$ and $\boldsymbol{\Delta}^- = [1, 2]^T$. This problem is solved in approximately 1 s and yields $\delta \in [-1.857, -1.857]$. In this instance, the reported upper and lower bound coincide because a feasible solution is found in the lower-bounding problem.

The low dimensionality of the problem allows us to visualize the results. for the final values for the generator set-points I_{g1}^0 and I_{g2}^0. The outcome is shown in Fig. 5 together with the optimized hyperbox of manageable uncertainties. We see that in this example and for the final values of the preventive actions (i.e., the generator set-points), the actual region of manageable uncertainties is a convex set, but we want to emphasize this does not hold in general.

The simple scaled hyperbox parameterization allows for an easily interpretable result and allows for faster computation compared to other parameterizations, such as a box where all dimensions are scaled individually. However, the visualization also shows that the result is conservative, i.e., the set of manageable uncertainties is significantly larger than the set of uncertainties guaranteed to be manageable according to the result of the computation.

In cases where a better approximation of the region of manageable uncertainties is desired, a possible improvement could be to *optimize* with a simple parametrization such as the scaled hyperbox and then *evaluate* for fixed preventive action for another, less conservative parameterization.

8.2 Small-scale instance

As a small-scale instance, we use the grid instance derived in (Djelassi et al. 2018) based on the 30-bus IEEE system. Figure 6 shows the topology of the grid. The main modifications compared to the 30-bus IEEE system are the introduction of three PSTs and the splitting of 7 nodes that are then subject to the bus merging. In (Djelassi et al. 2018), it was shown that if injections at non-generator nodes are considered to be uncertain within a range of ±30% of the nominal injections, all uncertainty realizations are manageable. To avoid the situation where the algorithm finishes in the first iteration for the parametric uncertainty formulation in Sect. 7.2, we increased the range to ±45% and increased the upper generator bounds by a factor of 1.13 to avoid a violation of (9). Table 1 summarizes key properties of this grid instance.
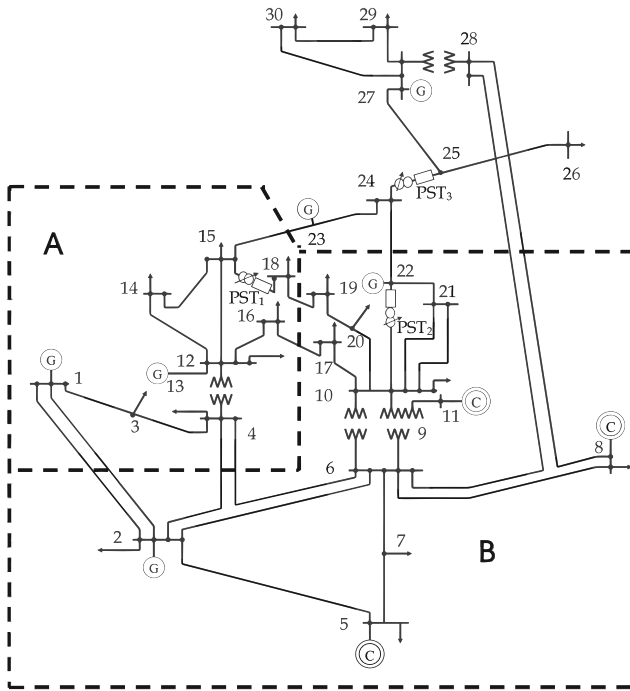
Fig. 6 Visualization of the small grid instance with two regions marked

8.2.1 Influence of α

We investigate the influence of the value of parameter α in (12f) on the solution time.

The selected worst-case uncertainty values y^*, i.e., the solutions to the maxmin problem (12f) that are used as discretization points, are selected according to two objectives. The parameter α weights the two objectives $\delta - h(x, y^*)$ and $\min_{z \in \mathcal{Z}(x, y^*)} g(x, y^*, z)$. The first can be understood to measure how far the discretization point y^* is inside the parametric uncertainty region $\mathcal{T}(\delta, x)$, while the second can be understood to measure the maximum violation considering the available control variables. For very small values of α, the overall objective will be determined more by the first objective.

The value of g in (17) is already normalized. In the following, we will choose $\alpha = \alpha'/\delta^{norm}$ to achieve a similar effect. For the parametrization of Sect. 7.1, we use $\delta^{norm} = 1$ and for the parametrization of Sect. 7.2 we use choose δ^{norm} as the optimistic value for δ, i.e., the value obtained when the uncertain injections would also become decision variables.

Tables 2 and 3 shows the range of wall times on the small grid instance for different values of α', for the parametrization from Sect. 7.1 and Sect. 7.2, respectively, for different configurations of the algorithm. The time range given is taken over three repetitions.

Table 2 Range of wall run times in seconds for the small grid instance with the parametrization from Sect. 7.1 for different values of α'. TIME_OUT denotes that the run-time limit of 3600 s was exceeded. The best time is given in bold font. If any of the proposed specializations is not used, this leads to a significant increase in computational time. for at least one value of α'. Run times vary strongly with α'

α'	All	Without auxiliary problem	Without dropping points	Without transformation
0.1	TIME_OUT	TIME_OUT	TIME_OUT	TIME_OUT
0.5	50–53	2850–2855	357–362	**34–35**
1	**77-80**	136–138	195–199	1181–1194
2	599–608	580–582	956–960	**122–126**
10	163–165	149–150	**25–27**	TIME_OUT

Table 3 Range of wall run times in seconds for the small grid instance with the parametrization from Sect. 7.2 for different values of α'. TIME_OUT denotes that the run-time limit of 3600 s was exceeded. The best time is given in bold font. Not using the proposed specializations of solving the auxiliary problem consistently leads to a significant increase in computational time for at least one value of α'. Run times vary strongly with α'

α'	All	Without auxiliary problem
0.05	**1228–1234**	1714–1838
0.1	**587–618**	1106–1186
0.5	**819–825**	2145–2247
1	TIME_OUT	TIME_OUT
2	TIME_OUT	TIME_OUT
10	TIME_OUT	TIME_OUT

We observe that the run time is strongly affected by the value of α', where the run time can more than double from one choice of α' to the next. This phenomenon is independent of the application of the algorithmic specializations from Sect. 6.3.

For the box parameterization, there does not seem to be a common good choice of α' between the different variants of the proposed algorithm. There is also no configuration that consistently outperforms the others. However, the variant using all the proposed specializations seems to be the most consistent over the different values of α', with the others having one value of α' where they take much longer than the other configurations. Not using the transformation specialization is either very beneficial, with it being the fastest approach, or leads to extremely increased computation times. Clearly, forgoing the transformation for simpler subproblems can be beneficial if the number of iterations stays low. We were surprised to find that for some values of α', not solving the auxiliary problem was faster, even though its computation was run in parallel. However, it turns out that in those instances, the auxiliary problem did simply not matter in terms of needed iterations and that the additional time was spent waiting for the abortion of the solution process of the auxiliary problem. This could potentially be prevented with a more forceful termination procedure. For the parameterization from

Table 4 Properties of the medium grid instance

Nodes	Generators	Edges	Shifters	Critical edges	Bus merges
6800	32	9,398	2	263	0

Sect. 7.2, where the run times were generally longer, using the auxiliary problem was always beneficial.

Overall, the algorithmic framework exhibits a significant inherent variation in run time with variations in α and similarly P^{lim}. This is due to the complex alteration of solution paths caused by the strong dependence of one subproblem solution on the sequence of earlier subproblem solutions.

Still, further research to explore whether an optimal static value of α for a given problem can be determined in advance or if adapting α during the algorithm execution would be beneficial.

In the absence of a systematically good choice, we choose $\alpha' = 0.5$ for the small grid instance.

8.2.2 Results

First, we use the parametrization from Sect. 7.2 in formulation (1) to compute the maximal additional power transfer capacity from part A to B of the network for the specified uncertainty ranges of $\pm 45\%$ of the nominal injections. The regions A and B are shown in the Fig. 6. Using $\alpha' = 0.5$, we terminate with $\delta \in [0.590\text{M W}, 0.614\text{M W}]$ after approximately 780 s using 18 iterations of the lower- and 16 iterations of the upper-bounding procedure, respectively. For comparison, the optimistic bound obtained when considering the uncertain injections also as decision variables is given by $\delta_{nom} = 0.863\text{M W}$.

Second, we use the parametrization from Sect. 7.1 with $\boldsymbol{\Delta}^+$ and $\boldsymbol{\Delta}^-$ chosen such that $\delta = 1$ represents the aforementioned $\pm 45\%$ deviation of the nominal injections. Using $\alpha' = 0.5$ yields a flexibility index $\delta \in [0.925, 0.954]$ in 12 iterations of the lower and the upper-bounding procedure, respectively, and approximately 63 s. We can thus guarantee that uncertainties at around 41% of the nominal injections can be handled. Repeating the computation of the maximal additional power transfer capacity for this reduced amount of uncertainty (41% instead of 45%), we obtain a capacity of 0.798M W. In this case, optimizing with a lower amount of uncertainty allows for a larger guaranteed available power transfer.

8.3 Medium-scale instance

The medium-scale models the power transmission grid over France and neighboring countries. Case files are accessible at (Zingler and Fliscounakis 2021). In our case study, we simulate a situation where uncertain injections in Spain are to be handled by generators in France. All uncertain injections except for one are situated in Spain and all active generators ($g \in G$ with $c_g \neq 0$) are situated in France and we want

to maximize the maximal additional power transfer capacity from France to Spain. The grid instance also contains nodes situated in other countries, but these do not contain active generators or uncertain injections. An overview over the properties of the instance is given in Table 4.

8.3.1 Results

Using $\alpha' = 10$ and the parametrization from Sect. 7.2, we obtain a maximal flow of approximately $\delta \in [4530\text{M W}, 4760\text{M W}]$ in approximately $300\,\text{s}$ in 3 iterations of the lower- and 2 of the upper-bounding procedure. The guaranteed maximal flow is close to the optimistic bound $\delta_{nom} = 4767\text{M W}$ obtained when considering the uncertain injections also as decision variables. As another point of reference, the total range of generation available for load distribution ($\sum_{g \in \mathcal{G}: c_g > 0} I_g^{x+} - I_g^{x-}$) is 8230M W. Here, we see that if only a small number of iterations is required until convergence, even large instances can be solved quickly.

For the parametrization from Sect. 7.1 and using $\alpha' = 10$, we obtain $\delta \in [0.546, 0.573]$ in approximately $83\,\text{min}$ with 17 iterations of the lower and 18 iterations of the upper-bounding procedure. As expected, the computational time required for the medium-scale instance is significantly larger than for the small-scale instance if a similar number of iterations is needed. Still, because we can utilize sophisticated MILP solvers for the subproblems, the problem can be solved in a reasonable amount of time. Repeating the computation of the maximal additional power transfer capacity for the reduced amount of uncertainty, we obtain a maximal additional power transfer capacity of 2600M W. In this case, directly optimizing for it allowed for a larger maximal additional power transfer capacity.

9 Conclusion

We formulated the maximization of the robustness of power grid operation as a hierarchical optimization problem, following the flexibility concept from process systems engineering (Grossmann et al. 1983). The formulation is rigorous in that it treats the uncertainty explicitly, but the resulting problem requires special solution methods.

For the solution, we specialized a discretization algorithm for existence-constrained semi-infinite optimization problems based on (Mitsos 2011). This allows us to include integer variables in the control variables and the uncertainty, for example, to describe piecewise linear functions. In the context of our grid model, which is based on the DC flow approximation, it also requires only the solution of mixed-integer linear optimization problems, which allows us to utilize commercial MILP solvers. As a result, numerical experiments on a medium-sized grid instance were shown to be solvable in reasonable computation times.

However, we have seen that the solution times can be high even for small grid instances and vary drastically with different choices of the scaling parameter α. For larger instances, the already rather high computational cost prohibits systematically testing different values. Further research is needed if robust choices for the algorithmic parameters can be found prior to solving the problem.

To illustrate the usefulness of the flexibility framework, we looked at two different interpretations of flexibility for power systems. The problem of finding a maximal available power transfer capacity between two parts of the network and finding the maximal manageable uncertainty when parametrized as a hyperbox. We showed results on a small and medium-scale power grid instance.

The presented methodology can be adapted to other parametrizations for the uncertainty region, as long as the defining function h is continuous. In the results of the medium-sized instance, we have illustrated that this can be vital: simply optimizing the flexibility in terms of a scaled hyperbox allows us to also guarantee flexibility in terms of maximal additional power transfer capacity for the reduced amount of uncertainty, but despite reducing the host set of the uncertainty, this yielded worse flexibility than optimizing it directly on the original host set of values for the uncertainties.

In the present work, we only considered the DC flow approximation. We rigorously consider the worst-case under this assumption, but if the real grid exhibits significant nonlinear behavior, this will likely be missed in our model. Another more accurate model could, at least in principle, be used, as long as the grid state is uniquely determined by the preventive actions x, the uncertain values y and the controls z. Although the computational effort can be expected to increase, the application to small grid instances seems tractable. Beyond that, future improvements could enable medium-sized instances for nonlinear models.

In conclusion, we believe that the presented methodology constitutes a valuable approach for increasing the robustness and reliability of power grids, today for DC flow approximation and in the future for nonlinear models.

Declarations

Conflict of interest The authors declare that they have no Conflict of interest.

Ethics approval and consent to participate (Not applicable)

Consent for publication No individual person's data is included, aside from the names and affiliations of the authors.

References

Akrami A, Doostizadeh M, Aminifar F (2019) Power system flexibility: an overview of emergence to evolution. J Mod Power Syst Clean Energy 7(5):987–1007. https://doi.org/10.1007/s40565-019-0527-4

Babatunde OM, Munda JL, Hamam Y (2020) Power system flexibility: a review. Energy Rep 6:101–10. https://doi.org/10.1016/j.egyr.2019.11.048

Blankenship JW, Falk JE (1976) Infinitely constrained optimization problems. J Opt Theory Appl 19(2):261–328. https://doi.org/10.1007/bf00934096

Bucher MA, Delikaraoglou S, Heussen K, Pinson P, Andersson G (2015) On quantification of flexibility in power systems. In: 2015 IEEE Eindhoven Power Tech, IEEE, pp 1. https://doi.org/10.1109/ptc.2015.7232514

Capitanescu F (2021) Power system flexibility region under uncertainty with respect to congestion and voltage constraints. In: 2021 IEEE Madrid Power Tech, IEEE, pp 1. https://doi.org/10.1109/powertech46648.2021.9494935

Djelassi H (2020) Discretization-based algorithms for the global solution of hierarchical programs. Dissertation, Rheinisch-Westfälische Technische Hochschule Aache. https://doi.org/10.18154/RWTH-2020-09163

Djelassi H, Mitsos A (2017) A hybrid discretization algorithm with guaranteed feasibility for the global solution of semi-infinite programs. J Global Opt 68(2):227–325. https://doi.org/10.1007/s10898-016-0476-7

Djelassi H, Mitsos A (2021) Global solution of semi-infinite programs with existence constraints. J Optim Theory Appl 188(3):863–883. https://doi.org/10.1007/s10957-021-01813-2

Djelassi H, Fliscounakis S, Mitsos A, Panciatici P (2018) Hierarchical programming for worst-case analysis of power grids. In: 2018 power systems computation conference (PSCC), IEEE, pp 1. https://doi.org/10.23919/pscc.2018.8444136

Djelassi H, Glass M, Mitsos A (2019) Discretization-based algorithms for generalized semi-infinite and bilevel programs with coupling equality constraints. J Global Opt 75(2):341. https://doi.org/10.1007/s10898-019-00764-3

Falk JE, Hoffman K (1977) A nonconvex max-min problem. Naval Res Logist Q 24(3):441–445. https://doi.org/10.1002/nav.3800240307

Gómez JD, Borda CE (2019) Operational flexibility in power systems-a geometrical view. In: 2019 IEEE power and energy society general meeting (PESGM), IEEE, pp 1. https://doi.org/10.1109/pesgm40551.2019.8974032

Grossmann IE, Floudas CA (1987) Active constraint strategy for flexibility analysis in chemical processes. Comput Chem Eng 11(6):675–679. https://doi.org/10.1016/0098-1354(87)87011-4

Grossmann IE, Halemane KP, Swaney RE (1983) Optimization strategies for flexible chemical processes. Comput Chem Eng 7(4):439–446. https://doi.org/10.1016/0098-1354(83)80022-2

International Energy Agency (2011) Harnessing variable renewables: a guide to the balancing challenge, OEC. https://doi.org/10.1787/9789264111394-en

Lee D, Turitsyn K, Molzahn DK, Roald LA (2021) Robust ac optimal power flow with robust convex restriction. IEEE Trans Power Syst 36(6):4953–4966. https://doi.org/10.1109/tpwrs.2021.3075925

Ma J, Silva V, Belhomme R, Kirschen DS, Ochoa LF (2013) Evaluating and planning flexibility in sustainable power systems. In: 2013 IEEE power and energy society general meeting, IEEE, pp 1–1. https://doi.org/10.1109/tste.2012.2212471

Menemenlis N, Huneault M, Robitaille A (2011) Thoughts on power system flexibility quantification for the short-term horizon. In: 2011 IEEE power and energy society general meeting, IEEE, pp 1. https://doi.org/10.1109/pes.2011.6039617

Mitsos A (2011) Global optimization of semi-infinite programs via restriction of the right-hand side. Optimization 60(10–11):1291–1301. https://doi.org/10.1080/02331934.2010.527970

Mitsos A, Tsoukalas A (2015) Global optimization of generalized semi-infinite programs via restriction of the right hand side. J Global Opt 61(1):1–10. https://doi.org/10.1007/s10898-014-0146-6

Nosair H, Bouffard F (2015) Flexibility envelopes for power system operational planning. IEEE Trans Sust Energy 6(3):800–805. https://doi.org/10.1109/tste.2015.2410760

Still G (1999) Generalized semi-infinite programming: Theory and methods. Eur J Oper Res 119(2):301–311. https://doi.org/10.1016/s0377-2217(99)00132-0

Wei-qing S, Cheng-min W, Yan Z (2012) Flexibility evaluation and flexible comprehensive optimization in power systems. Eur Trans Electr Power 22(6):846–867. https://doi.org/10.1002/etep.617

Zhao F, Ochoa MP, Grossmann IE, García-Muñoz S, Stamatis SD (2022) Novel formulations of flexibility index and design centering for design space definition. Comput Chem Eng 166:10796. https://doi.org/10.1016/j.compchemeng.2022.107969

Zhao J, Zheng T, Litvinov E (2015) A unified framework for defining and measuring flexibility in power system. IEEE Trans Power Syst 31(1):339–347. https://doi.org/10.1109/TPWRS.2015.2390038

Zingler A, Fliscounakis S (2021) Medium-scale power grid instance with 6800 nodes for DC-flow approximation. https://publications.rwth-aachen.de/record/828516